atmosphere

MDPI

Article

The Zonal Wind Intraseasonal Oscillation in the Exit Region of the East Asian Subtropical Westerly Jet in Winter and Its Thermodynamic Mechanism

Suxiang Yao * and Yishan Liu

Key Laboratory of Meteorological Disaster, Ministry of Education/Collaborative Innovation Center on Forecast and Evaluation of Meteorological Disasters, Nanjing University of Information Science and Technology, Nanjing 211544, China; 20191201050@nuist.edu.cn

* Correspondence: yaosx@nuist.edu.cn

Abstract: The six-hourly ERA-interim reanalysis data were used to analyze the intraseasonal oscillation (ISO) characteristics of the zonal wind in the exit region of the East Asian subtropical westerly jet (EAJ) during the winter (November to April). The results indicate that from East Asia to the North Pacific, the zonal wind in the upper troposphere shows significant 10–40-day oscillations, propagating eastward toward the jet exit region. The strength of the intraseasonal zonal wind anomaly increases from the lower troposphere to the upper troposphere, reaching a peak between 300 and 200 hPa. The zonal wind ISO in the jet exit area is closely related to the intraseasonal inverse temperature tendency between the north and south of the jet exit in the troposphere. In the acceleration (deceleration) phase of the intraseasonal west wind, the air temperature decreases (increases) in the north of the exit and increases (decreases) in the south of the exit. The intraseasonal temperature tendency is stronger in the north of the EAJ exit than that in the south. In the north of the EAJ exit, the intraseasonal temperature tendency is decided by the temperature advection, where the whole troposphere is controlled by the north wind in the west wind acceleration phase and controlled by the south wind in the west wind deceleration phase, so the intensity of temperature advection is strong. However, adiabatic heating plays a decisive role in affecting the temperature evolution in the south of the jet exit area, and the intraseasonal meridional wind is the opposite between the mid-upper troposphere and the lower troposphere, resulting in weak temperature advection and the weak temperature tendency. Therefore, although the zonal wind ISO in the jet exit area is the result of the joint action of the ISOs in different latitudes, the influence of mid-high latitudes is particularly important.

Keywords: intraseasonal oscillation; subtropical westerly jet; temperature advection; adiabatic heating

Citation: Yao, S.; Liu, Y. The Zonal Wind Intraseasonal Oscillation in the Exit Region of the East Asian Subtropical Westerly Jet in Winter and Its Thermodynamic Mechanism. *Atmosphere* **2022**, *13*, 395. https://doi.org/10.3390/atmos13030395

Academic Editor: Massimiliano Burlando

Received: 10 February 2022
Accepted: 26 February 2022
Published: 27 February 2022

1. Introduction

Since Madden and Julian [1,2] identified intraseasonal atmospheric oscillations in the 1970s, broad studies have been conducted, especially on tropical ISOs. In particular, a good understanding of the structural characteristics and activity patterns of the Madden-Julian oscillation [3–6] has been developed. However, studies of ISOs in subtropical regions remain relatively scarce.

Subtropical westerly jets are strong and narrow global westerlies that appear in the subtropical upper troposphere with central zonal winds greater than 30 m/s. The horizontal length reaches a few tens of thousands of kilometers, and the width is a few hundred kilometers [7]. The EAJ has important effects on the weather and climate in East Asia and the Pacific Ocean [8–11]. Studies have shown that jets are mainly generated by the dynamic and thermal effects of huge mountains [12,13], land-ocean thermal contrasts, tropical convection, latent heat due to subtropical precipitation [14,15], large-scale angular momentum transport in vortices, and wave-current interactions [16–20].

Previous studies have focused on the seasonal, interannual, and interdecadal variation characteristics of the EAJ. Tropical and subtropical precipitation and high-latitude circulation have important effects on the annual and decadal jet variations [21–23]. In recent years, high-resolution meteorological data have enabled researchers to study the intraseasonal variation in the EAJ [24]. The results show that the westerly jet is not only a simple "stable" planetary-scale system, but also displays strong intraseasonal variation [21,25,26]. Some studies report that in the subtropical Northern Hemisphere, the energies of the ISOs of zonal wind are concentrated to waves with a wave number of one and a period of 30–60 days, and the westward propagating energies for the 30–60-day oscillations are stronger than the eastward propagating energies [27]. Other studies have indicated that the polar vortex and the anomalous wave breaking in the mid-latitudes force the different timescales of the EAJ, including the intraseasonal variation [28]. Although it is generally accepted that westerly jets control subtropical precipitation, the latent heat released during subtropical precipitation can significantly enhance the strength of the EAJ by influencing the air temperature gradient [21,25,29].

Previous studies have shown that the zonal wind ISO near the jet core is not as strong as that in the jet entrance area [26]. However, it should be noted that the ISO of the geopotential height at the exit of the EAJ is significantly stronger than at the entrance [30]. Therefore, the question must be asked—is the ISO intensity of zonal wind consistent with that of geopotential height? Is there a strong zonal wind ISO in the jet exit region? In order to answer these questions, this paper focuses on the characteristics and evolution mechanism of zonal wind ISOs in the exit area of the EAJ. The remainder of this article is organized as follows: descriptions of the data and methods are presented in Section 2; in Section 3, the characteristics of the zonal wind ISO in the jet exit are first analyzed, and then the relationship between zonal wind ISOs and the meridional temperature gradient is given; finally, discussions and conclusions are presented in Sections 4 and 5, respectively.

2. Data and Methods

2.1. Data

The data used in this study are the six-hourly ERA-interim reanalysis data [31], which include the meridional wind, the zonal wind, the air temperature, and the vertical velocity at pressure levels (https://apps.ecmwf.int/datasets/data/interim-full-daily/levtype=pl/, accessed on 25 February 2022). The spatial resolution is 1.5° × 1.5°. We averaged the six-hourly data to obtain daily data.

This study selected the period from November of each year to April of the next year as the winter. From 1979/1980 to 2012/2013, there were 34 winters and 6163 days in total.

2.2. Methods

Power spectrum analysis was chosen to analyze the dominant period of the winter zonal wind. We used Butterworth band-pass filtering to obtain the ISO (10–40-day) and the synoptic-scale (<10 days) components of the variables, and used a Gaussian low-pass filter to obtain the background field (>40 days). Firstly, the data of 12781 days from 1979 to 2013 were filtered, and then the 6163 days in winter were selected for analysis.

The thermal wind principle was projected [32] onto an intraseasonal (10–40-day) scale (Equation (1)), where a superscript prime indicates 10–40-day filtering, u represents the zonal wind, p represents the pressure, R is the gas constant, f is the Coriolis parameter, and T is the air temperature.

$$(\frac{\partial u}{\partial p})' = (\frac{R}{fp})\frac{\partial T'}{\partial y} \quad (1)$$

In order to reveal the key process which influence the temperature, the first law of thermodynamics is used in this paper. The first law of thermodynamics dictates that

temperature tendency is primarily determined by the following three terms [32], as shown in Equation (2).

$$\frac{\partial T\prime}{\partial t} = -(\vec{V}\cdot\nabla T)\prime - (\omega(\frac{\partial T}{\partial p} - \frac{R}{C_p}\frac{T}{P}))\prime + \frac{Q\prime}{Cp} \quad (2)$$

The three terms on the right are the temperature advection (ADVT), adiabatic (ADIA) heating, and diabatic (DIA) heating. T, R, p are the same as in Equation (1). $\vec{V}$ is the wind vector. ω is the vertical velocity. C_p is the specific heat capacity. Q is the diabatic heating rate, where the diabatic heating is calculated as the following:

$$\frac{Q\prime}{C_p} = \frac{\partial T\prime}{\partial t} - (-(\vec{V}\cdot\nabla T)\prime - (\omega(\frac{\partial T}{\partial p} - \frac{R}{C_p}\frac{T}{P}))\prime) \quad (3)$$

Using the scale decomposition method [33] and letting any meteorological variable $A = \overline{A} + A' + A''$, the intraseasonal temperature advection can be decomposed to 18 terms as follows:

$$\begin{aligned}
-(\vec{V}\cdot\nabla T)\prime \quad = \quad & \underbrace{-(\overline{u}\frac{\partial\overline{T}}{\partial x})\prime}_{\text{advt1}} \quad \underbrace{-(\overline{u}\frac{\partial T\prime}{\partial x})\prime}_{\text{advt2}} \quad \underbrace{-(\overline{u}\frac{\partial T''}{\partial x})\prime}_{\text{advt3}} \quad \underbrace{-(u\prime\frac{\partial\overline{T}}{\partial x})\prime}_{\text{advt4}} \quad \underbrace{-(u\prime\frac{\partial T\prime}{\partial x})\prime}_{\text{advt5}} \quad \underbrace{-(u\prime\frac{\partial T''}{\partial x})\prime}_{\text{advt6}} \quad \underbrace{-(u''\frac{\partial\overline{T}}{\partial x})\prime}_{\text{advt7}} \quad \underbrace{-(u''\frac{\partial T\prime}{\partial x})\prime}_{\text{advt8}} \quad \underbrace{-(u''\frac{\partial T''}{\partial x})\prime}_{\text{advt9}} \\
& \underbrace{-(\overline{v}\frac{\partial\overline{T}}{\partial y})\prime}_{\text{advt10}} \quad \underbrace{-(\overline{v}\frac{\partial T\prime}{\partial y})\prime}_{\text{advt11}} \quad \underbrace{-(\overline{v}\frac{\partial T''}{\partial y})\prime}_{\text{advt12}} \quad \underbrace{-(v\prime\frac{\partial\overline{T}}{\partial y})\prime}_{\text{advt13}} \quad \underbrace{-(v\prime\frac{\partial T\prime}{\partial y})\prime}_{\text{advt14}} \quad \underbrace{-(v\prime\frac{\partial T''}{\partial y})\prime}_{\text{advt15}} \quad \underbrace{-(v''\frac{\partial\overline{T}}{\partial y})\prime}_{\text{advt16}} \quad \underbrace{-(v''\frac{\partial T\prime}{\partial y})\prime}_{\text{advt17}} \quad \underbrace{-(v''\frac{\partial T''}{\partial y})\prime}_{\text{advt18}}
\end{aligned} \quad (4)$$

Also, the adiabatic heating can be decomposed to 9 terms:

$$\begin{aligned}
-(\omega(\tfrac{\partial T}{\partial p} - \tfrac{R}{C_p}\tfrac{T}{P}))\prime = \quad & \underbrace{-(\overline{\omega}(\tfrac{\partial\overline{T}}{\partial p} - \tfrac{R}{C_p}\tfrac{\overline{T}}{P}))\prime}_{ADIA1} \quad \underbrace{-(\overline{\omega}(\tfrac{\partial T\prime}{\partial p} - \tfrac{R}{C_p}\tfrac{T\prime}{P}))\prime}_{ADIA2} \quad \underbrace{-(\overline{\omega}(\tfrac{\partial T''}{\partial p} - \tfrac{R}{C_p}\tfrac{T''}{P}))\prime}_{ADIA3} \quad \underbrace{-(\omega\prime(\tfrac{\partial\overline{T}}{\partial p} - \tfrac{R}{C_p}\tfrac{\overline{T}}{P}))\prime}_{ADIA4} \\
& \underbrace{-(\omega\prime(\tfrac{\partial T\prime}{\partial p} - \tfrac{R}{C_p}\tfrac{T\prime}{P}))\prime}_{ADIA5} \quad \underbrace{-(\omega\prime(\tfrac{\partial T''}{\partial p} - \tfrac{R}{C_p}\tfrac{T''}{P}))\prime}_{ADIA6} \quad \underbrace{-(\omega''(\tfrac{\partial\overline{T}}{\partial p} - \tfrac{R}{C_p}\tfrac{\overline{T}}{P}))\prime}_{ADIA7} \quad \underbrace{-(\omega''(\tfrac{\partial T\prime}{\partial p} - \tfrac{R}{C_p}\tfrac{T\prime}{P}))\prime}_{ADIA8} \quad \underbrace{-(\omega''(\tfrac{\partial T''}{\partial p} - \tfrac{R}{C_p}\tfrac{T''}{P}))\prime}_{ADIA9}
\end{aligned} \quad (5)$$

In the above equations, the over bars represent the results of low-pass filtering on a time scale that is greater than 40 days, which comprise the background field. The superscript prime represents 10–40-day bandpass filtering results, which comprise the ISO component, and the double prime represents the synoptic scale component, which is the results of 3–10-day bandpass filtering.

3. Results

3.1. The Characteristics of the Zonal Wind ISO at the Jet Exit

Figure 1a shows the mean zonal wind at 200 hPa in the winter and its mean square deviation. The zonal wind of the EAJ core exceeds 60 m/s. The jet's axis is between 25° N and 35° N. The jet core is near Japan. The mean square deviation of the zonal wind is strongest at the exit of the jet over the Pacific (170° E–150° W, 30° N–40° N, green box in Figure 1a), where the strength exceeds 18 m/s, which is much greater than the 14 m/s in the jet entrance area region. The mean square deviation distribution of zonal wind and zonal wind at 500 hPa (Figure 1b) is similar to that at 200 hPa, but the strength is much weaker than that at 200 hPa. Using the method of power spectrum analysis, the dominant period of zonal wind in the exit area of the jet at 200 hPa was analyzed (Figure 1c). It was found that 95% of the red noise test was passed on a scale of 10–40 days. The mean square deviation of the 10–40-day filtered zonal wind is shown in Figure 1d. The mean square deviation of the intraseasonal zonal wind in the jet exit region was more than 9 m/s, which is much greater than that in the entrance area of the jet and the jet core. The ISO variance accounts for about 50% of the total variance. Therefore, the exit area of the EAJ has a very significant intraseasonal variability, and its dominant period is 10–40 days.

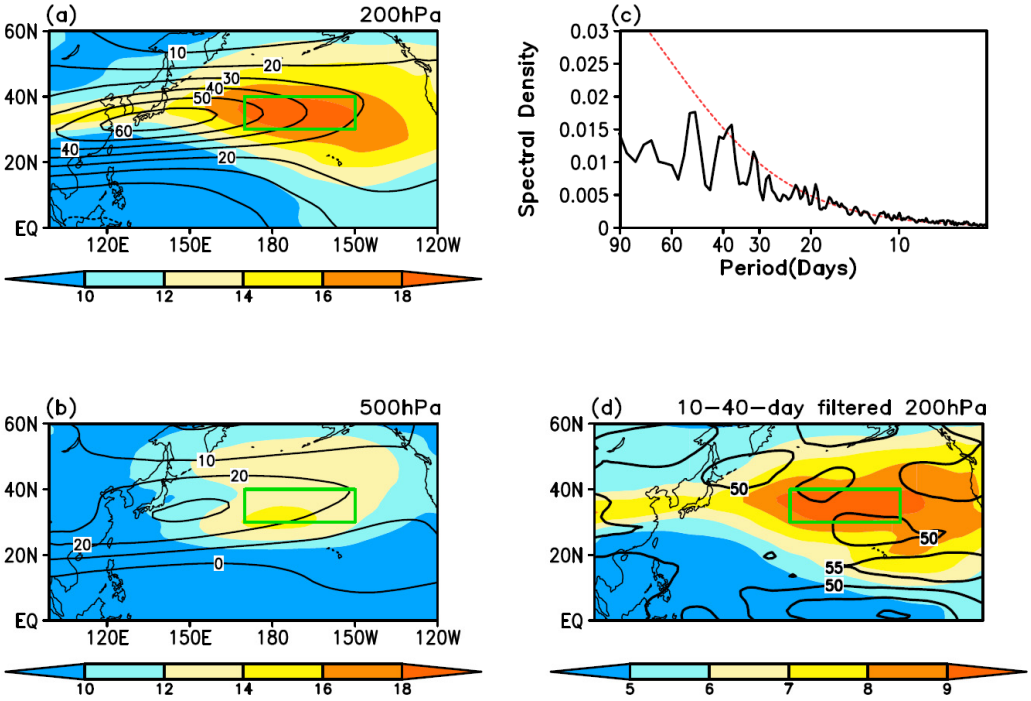

Figure 1. The mean zonal wind (contour, unit: m/s) and its mean square deviation (color shades, unit: m/s) in winter ((**a**): 200 hPa, (**b**): 500 hPa), power spectrum analysis of the zonal wind in the exit region at 200 hPa (**c**), the mean square deviation of intraseasonal zonal wind (color shades, unit: m/s) and the total variances explained by the ISO (contour, unit: %) at 200 hPa (**d**). The green box represents the jet exit region (170° E–150° W, 30° N–40° N), the red dashed line the 95% red noise test, and the black solid line the power spectral density.

Further, the zonal wind in the exit area of the EAJ was filtered, and the intraseasonal component of 10–40-day was obtained. When the peak value of intraseasonal (10–40-day filtered) zonal wind (including easterly and westerly) was greater than one standard deviation, it was defined as an oscillation event of zonal wind. In the 34 winters from 1979/1980 to 2012/2013, a total of 107 positive oscillation events (the peak of the intraseasonal wind anomaly was westerly) and 118 negative oscillation events (the peak of the intraseasonal wind anomaly was easterly) occurred. We first analyzed the temporal evolution of the zonal wind ISO at the exit (Figure 2). Day 0 denotes the peak day of the 10–40-day filtered zonal wind at the exit of the EAJ. Day −3 denotes 3 days before the peak day, and day 3 represents 3 days after the peak day, and so on. Analysis revealed that the positive and negative events all have a dominant period of approximately 18 days. The maximum intraseasonal westerly and easterly anomalies are greater than 12 m/s. The positive events and negative events are symmetrically distributed and occur with similar frequency. Therefore, in the following analysis, we did not analyze the positive and negative events separately but rather discussed the difference between them.

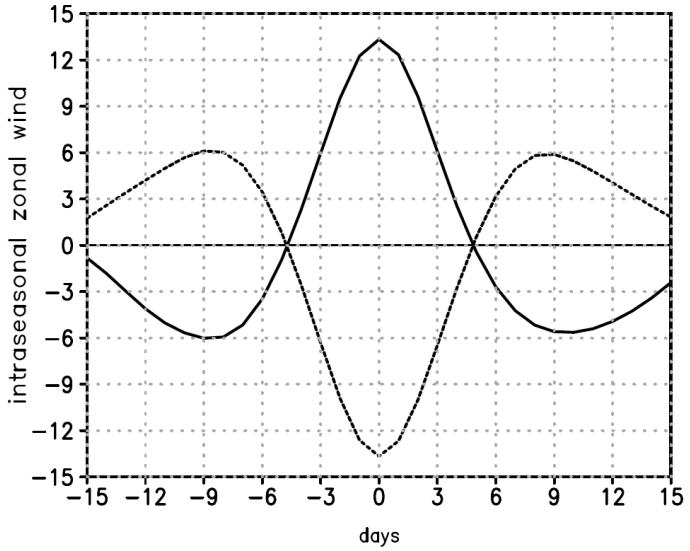

Figure 2. Composite of the intraseasonal zonal wind evolution at 200 hPa based on the zonal wind ISO events in the jet exit region (unit: m/s). The solid line is the synthetic result of the positive events. The dashed line is the synthetic result of the negative events. "0" in the abscissa represents the peak day of the positive (or negative) events. "−3" represents three days before the peak day, "3" represents three days after the peak day, and so on.

The spatial distribution and migration characteristics within one cycle (from day −9 to day 9) of the zonal wind ISO are shown in Figure 3. Nine days before the westerlies' peak day, the jet entrance and exit were out of phase (Figure 3a). The positive westerly anomaly center was located over China. The jet exit was controlled by a negative anomaly. The strength of the EAJ was weak, and the jet core was located in southern Japan. At day −6 (Figure 3b), the positive anomaly migrated eastward, the jet stream exit area was still controlled by easterly anomalies, and the intensity of the EAJ increased. At day −3 (Figure 3c), the intraseasonal west wind anomaly moved eastward to the exit area of the EAJ, which enhanced the intensity of the EAJ, as would be expected. On the peak day (Figure 3d), the intraseasonal westerly anomaly reached the strongest in the jet exit area, and the jet core reached the easternmost position. As for the jet exit region, from day −9 to day 0, the intraseasonal west wind accelerated, so there was an acceleration phase of west wind. At day 3 (Figure 3e), the intraseasonal west wind in the exit area of the EAJ was weakened, the intensity of the EAJ was also weakened, and the jet core moved westward. At day 6 and 9 (Figure 3f,g), the exit area of the jet turned to an intraseasonal easterly anomaly, the intensity of the jet weakened, and the jet core returned to southern Japan. From day 0 to day 9, there was a deceleration phase of west wind. In addition, the streamline displays an abnormal intraseasonal anti-cyclonic (cyclonic) circulation found to the north (south) of the anomalous easterlies, and an abnormal cyclonic (anti-cyclonic) circulation found to the north (south) of the anomalous westerlies.

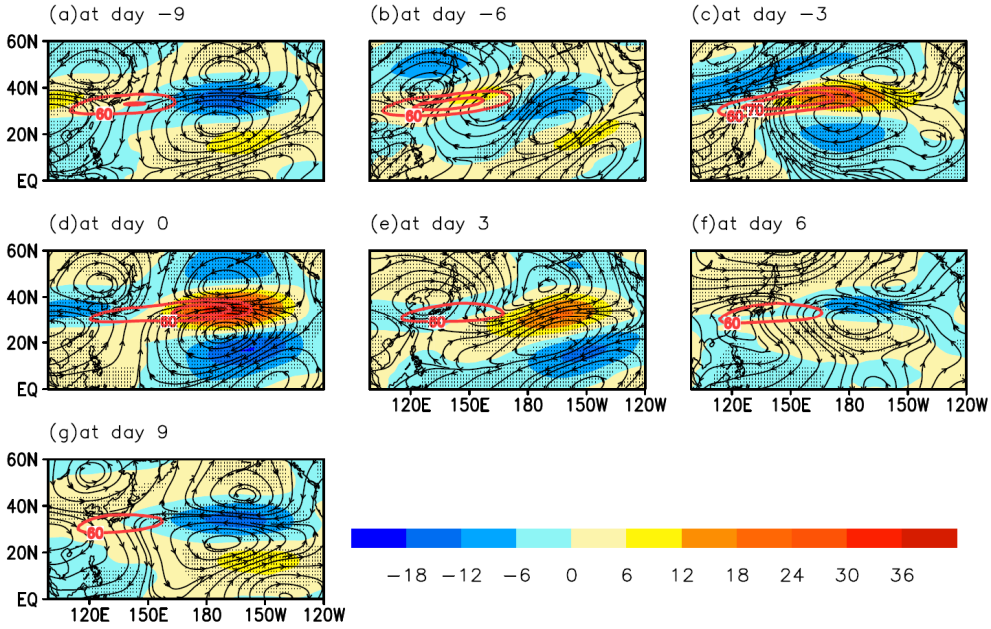

Figure 3. Composite of the intraseasonal zonal wind (color shade, unit: m/s), the intraseasonal air flow (stream line), and the zonal wind (only ≥60 m/s are shown, the red line, unit: m/s) at 200 hPa from day −9 to day 9 (**a**–**g**), with an interval of 3 days. The dotted area indicates that the intraseasonal zonal wind anomaly at 200 hPa passed the t-test with 95% confidence.

The above results give the horizontal distribution characteristics of the intraseasonal evolution of the zonal wind ISO at 200 hPa, and further analyze its vertical structure. Figure 4 shows the time-altitude profile diagram of the zonal wind and 10–40-day filtered zonal wind at the jet exit. From 1000 hPa to 30 hPa, the intraseasonal zonal wind experiences the processes of accelerating during day −9 to day 0, and then decelerating during day 0 to day 9, which has the same evolution as that at 200 hPa. The maximum oscillation center appears between 300 and 200 hPa, where the zonal wind (raw data, color shaded) is also strongest.

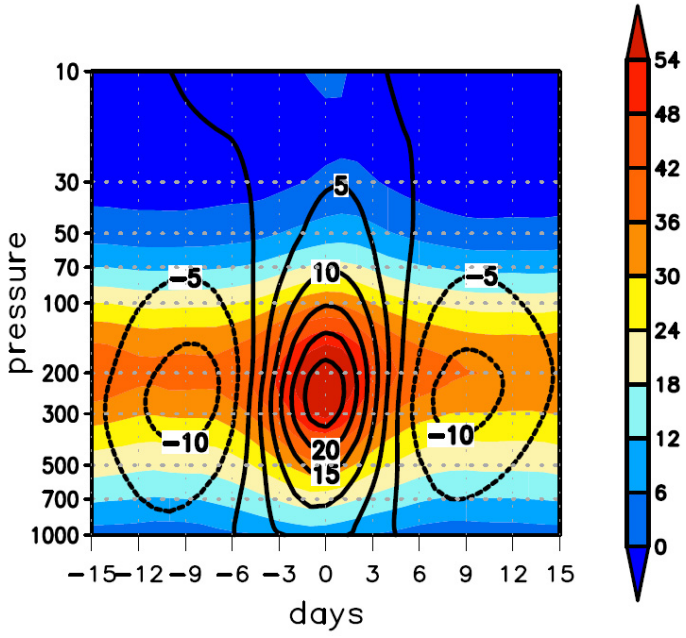

Figure 4. The time-altitude profile of the zonal wind (color shaded) and the intraseasonal zonal wind (contoured) in the jet exit region (unit: m/s).

In general, because of the spatial distribution of the tropospheric temperature (high in the south and low in the north) in the upper troposphere (at approximately 200 hPa), the westerlies reach their maximum strength because of the meridional temperature gradient [7]. The center of the maximum intraseasonal zonal wind oscillation is also in the upper troposphere. Therefore, it is necessary to analyze the intraseasonal temperature distribution in the troposphere associated with the zonal wind ISO at the jet exit.

3.2. Zonal Wind ISO and Intraseasonal Temperature Variation

Firstly, the vertical distribution characteristics of the intraseasonal temperature gradient ($\frac{\partial T\prime}{\partial y}$) in the exit area of EAJ were analyzed (Figure 5a). When the intraseasonal temperature gradient from 1000 to 300 hPa was negative ($\frac{\partial T\prime}{\partial y} < 0$, from day −4 to day 4), it was an intraseasonal west wind anomaly, corresponding to warm in the south and cold in the north. On a day with anomalous easterlies, it was cold in the south and warm in the north ($\frac{\partial T\prime}{\partial y} > 0$). The temperature gradient was strongest in the middle of the troposphere (at 600–400 hPa), and the gradient above 300 hPa was opposite to that below 300 hPa, which is the reason that the maximum oscillation of the westerlies appears at 300–200 hPa (Figure 4). At the peak day of the zonal wind oscillation, the temperature gradient was the strongest. The horizontal distributions of the 10–40-day filtered temperature and the temperature gradient integrated from 1000 to 300 hPa on the peak day are shown in Figure 5b. It is plain that the temperature in the North Pacific troposphere has a distribution that is warm in the south and cold in the north. The jet exit has the maximum intraseasonal temperature gradient. Anomalous intraseasonal warm and cold centers are distributed to the south (170° E–150° W, 20–30° N, blue box in Figure 5b) and north (170° E–150° W, 40–50° N, green box in Figure 5b) sides of the jet exit, respectively.

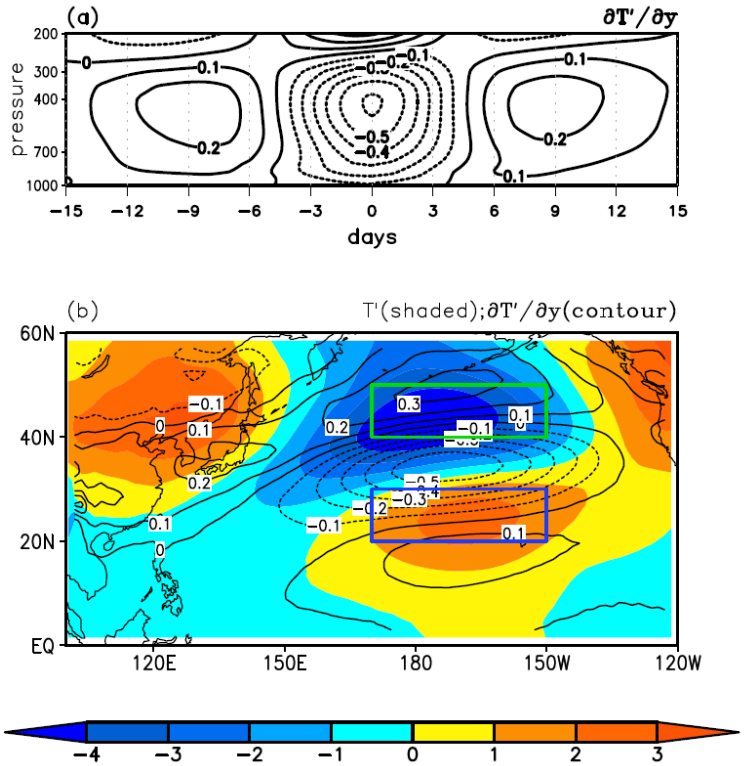

Figure 5. The time-altitude profile of the 10–40-day filtered temperature gradient in the jet exit region (**a**, unit: 10^{-5} °C/m), the 10–40-day filtered temperature (**b**, shaded, unit: °C), and the 10–40-day filtered temperature gradient (**b**, contoured, unit: 10^{-5} °C/m) synthesized on the peak day, integrated from the surface to 300 hPa. The green box represents the area north of the jet exit region (170° E–150° W, 40–50° N); the blue box represents the south of the jet exit region (170° E–150° W, 20°–30° N).

In order to explain the intraseasonal temperature variability, the 10–40-day filtered temperature tendency was further analyzed (Figure 6). In the acceleration phase of the intraseasonal west wind (day −9 to day 0), the north of the exit showed significant cooling (Figure 6a), while the south showed significant heating (Figure 6b). In the deceleration phase of the intraseasonal west wind (day 0 to day 9), the north of the exit showed significant heating (Figure 6a), while the south showed significant cooling (Figure 6b). The out-of-phase temperature tendency between the south and north caused the zonal wind oscillation.

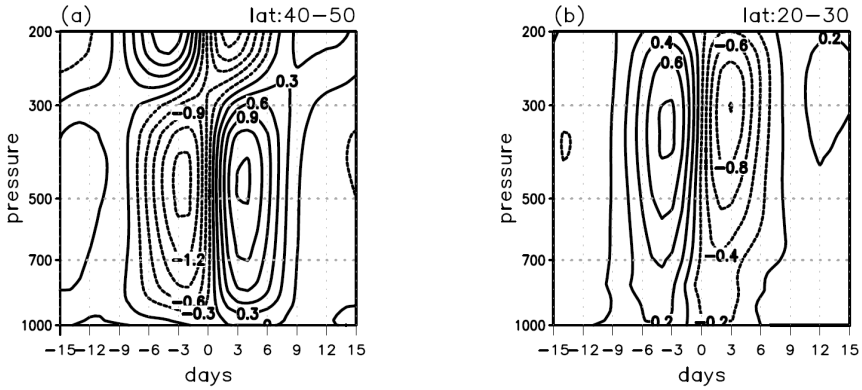

Figure 6. The time-altitude profile of the 10–40-day filtered temperature tendency in the north (**a**), and south (**b**) of the exit region. Unit: °C/d.

The temperature tendency (T-TED) depends on the temperature advection (ADVT), adiabatic (ADIA), and diabatic (DIA) terms (Equation (2)). Figure 7 shows the four terms integrated from the surface to 300 hPa on the intraseasonal scale. It is clear that the intraseasonal temperature tendency in the north is stronger than that in the south, and the adiabatic (ADIA) term always has a favorable influence on the temperature tendency on both sides of the jet exit. To the north of the exit, the largest contributor to the cooling (from day −9 to day 0) or the heating (from day 0 to day 9) is the air temperature advection (ADVT) (Figure 7a,b). To the south of the exit, the temperature advection is weak, and the adiabatic (ADIA) term contributes the most (Figure 7c,d).

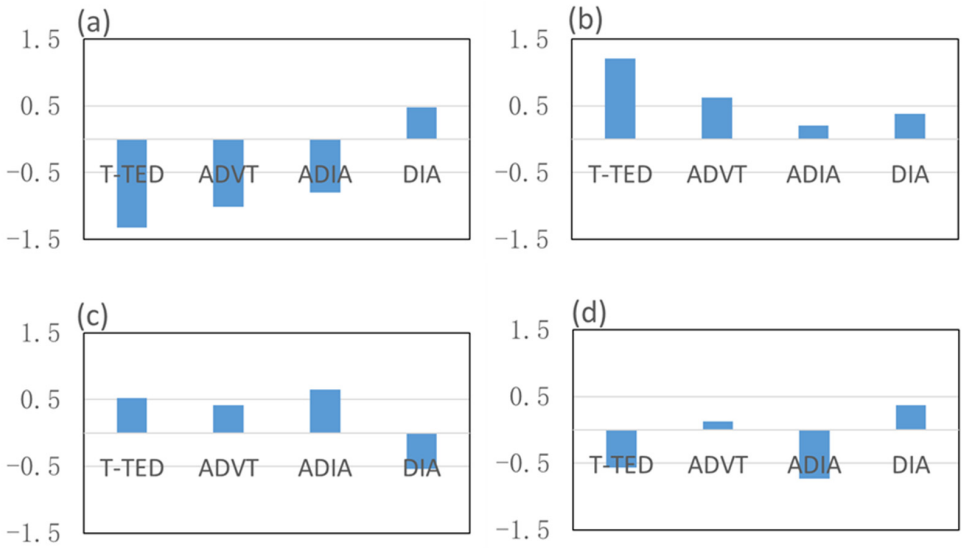

Figure 7. The 10–40-day filtered temperature tendency (T-TED), temperature advection (ADVT), adiabatic variation (ADIA), and diabatic variation (DIA) during the nine days before the peak day (**a**), and the nine days after the peak day (**b**) in the north of the jet exit region integrated from the surface to 300 hPa; (**c**) shows the nine days before the peak day in the south of the exit region; and (**d**) shows the nine days after the peak day in the south of the exit region. Unit: °C/d.

Further analysis of the temperature advection to the north of the exit is shown in Figure 8a based on Equation (4). Obviously, the 13th term $(-v\prime\frac{\partial\overline{T}}{\partial y})\prime$ in Equation (4) is the most important one during both the nine days before the peak day and the nine days after the peak day. In the north of the jet exit region, the intraseasonal meridional wind advects the background temperature (time scale > 40 days), which has an important influence on the intraseasonal temperature tendency, which then affects the zonal wind. As for the south of the jet exit, the adiabatic heating mainly depends on the intraseasonal vertical velocity and the mean temperature $(-(\omega'(\frac{\partial\overline{T}}{\partial p}-\frac{R}{C_p}\frac{\overline{T}}{P}))\prime)$ (Figure 8b).

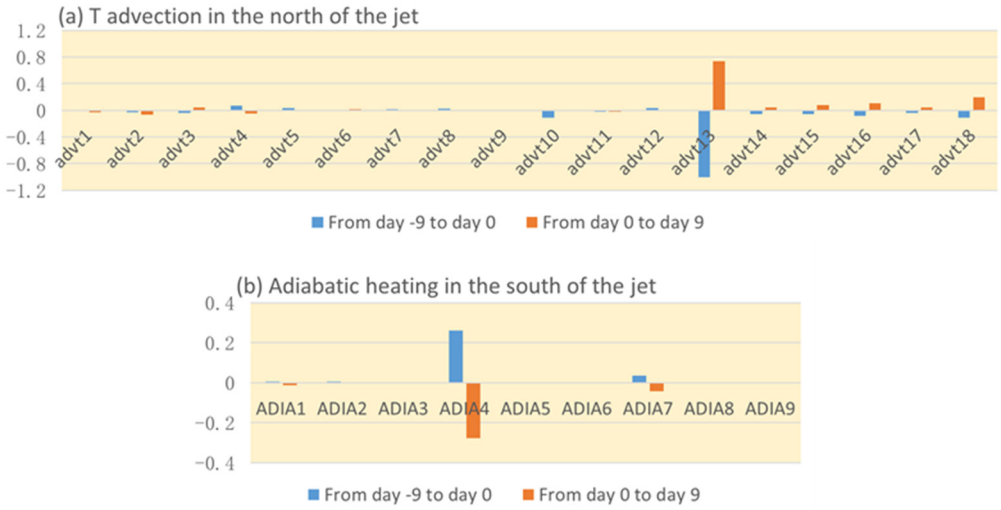

Figure 8. The 18 terms of the intraseasonal temperature advection based on Equation (4) in the north of the jet exit (**a**), and the 9 terms of the intraseasonal adiabatic heating based on Equation (5) in the south of the jet exit (**b**) integrated from the surface to 300 hPa. Unit: °C/d.

3.3. The Intraseasonal Meridional Circulation near the Jet Exit

The above analysis shows that the ISO of the zonal wind corresponds to the ISO of the temperature gradient, and the temperature anomalies depend on the intraseasonal meridional wind, vertical velocity, and background temperature. Therefore, the intraseasonal meridional circulation near the jet exit region was further analyzed. Figure 9 shows the latitude-altitude profile of the 10–40-day filtered meridional wind, vertical velocity, and background temperature near the jet exit area (170° E–150° W). During the westerly acceleration period (averaged from day −9 to day 0), ascending motion was found to the north of the jet exit and descending motion was found to the south of the jet exit (Figure 9a). To the north of the jet exit, the whole troposphere was a north wind anomaly. However, to the south of the jet exit area, the north wind anomaly was in the middle and upper troposphere, and the south wind anomaly was in the lower troposphere, which weakened the temperature advection. Therefore, from day −9 to day 0, the warming in the south was mainly due to the adiabatic heating caused by the sinking motion. From day 0 to day 9 (Figure 9b), the north of the jet exit area was mainly controlled by the south wind anomaly, accompanying a descending motion which is conducive to warming. An ascending motion anomaly occurred in the south of the jet exit area, corresponding to the adiabatic cooling. It is thus clear that the vertical meridional circulation near the EAJ exit is an important reason for the intraseasonal temperature gradients.

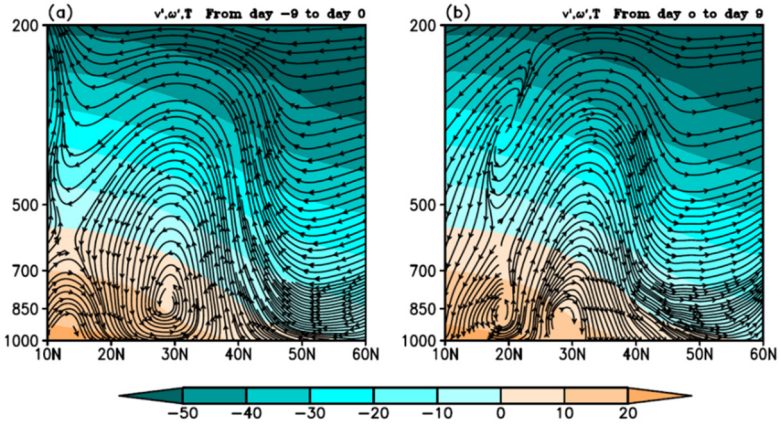

Figure 9. The 10–40-day filtered vertical meridional circulation averaged from 170° E to 150° W. The shading represents the mean temperature (time scale > 40 days) (unit: °C), and the streamline represents the intraseasonal meridional wind (unit: m/s) and vertical velocity (10^{-2} Pa/s). (**a**) shows the average from day −9 to day 0, (**b**) shows the average from day 0 to day 9.

4. Discussion

This paper analyzes the ISO characteristics and thermal mechanisms of the zonal wind in the exit area of the EAJ in winter. It was found that the ISO intensity of the zonal wind in the exit area is stronger than that in the entrance area. The results are interesting, and present a strong supplement to the relevant research [26]. Combined with the research of Yao et al. [30], it can be considered that the ISO strength of the potential height and the zonal wind at the jet exit is significantly stronger than that in the jet core and the jet entrance, and the North Pacific is a key area of ISO in the subtropical region.

It was also found that the winter zonal wind ISO in the exit area of the jet is related to the secondary meridional circulation near the jet exit, and is effected by both the atmospheric circulation in the mid-high latitudes and low latitudes. Therefore, in future studies, Madden-Julian oscillations and ISO in mid-high latitudes should be considered, especially the latter, because the intraseasonal temperature tendency to the north of the jet is significantly stronger than that to the south. Moreover, this paper only focuses on the zonal wind ISOs in winter. Whether this conclusion is applicable to the summer, and whether ISO is the dominant variability during the alternation of seasons, are questions worthy of further study.

5. Conclusions

The EAJ and its variance have important influences on temperature and precipitation in East Asia and the North Pacific. There is an obvious intraseasonal evolution in jet intensity and jet core location, and it is of great significance to study the ISO of the zonal wind near the jet. The six-hourly ERA-interim reanalysis data were used to analyze the ISO characteristics of the zonal wind from East Asia to the Pacific Ocean, and it was found that the zonal wind in the upper troposphere has the dominant period of 10–40 days. The strongest oscillation center was near the exit of the EAJ. The intraseasonal zonal wind propagated eastward and strengthened significantly at the jet exit, which also had influence on the strength of the EAJ and the position of the jet core. In the phase of intraseasonal west wind acceleration (deceleration) in the exit area, the intensity of EAJ was strong (weak), and jet core moved eastward (westward). Therefore, to study the evolution characteristics of jet, it may be necessary to focus on the ISO of zonal wind in its exit area.

The ISO of 200 hPa zonal wind depends on the intraseasonal meridional temperature gradient in the troposphere. The intraseasonal cooling (heating) in the north and warming (cooling) in the south are favorable for the strengthening (weakening) of west winds at the tropopause. The intraseasonal temperature evolution to the north of the EAJ exit mainly

depended on the temperature advection, while adiabatic heating related with the vertical motion played a decisive role in the temperature tendency south of the jet exit area.

The ISO of the zonal wind in the jet exit area was accompanied by the oscillation of the meridional circulation. During the period of the intraseasonal westerly acceleration (deceleration), there was a north (south) wind anomaly near the jet exit area. To the north of the jet exit area, the whole troposphere presented a north wind (south wind) anomaly, and thus was controlled by strong cold (warm) advection. However, to the south of the exit area, there was a north (south) wind anomaly at the mid-high troposphere and a south (north) wind anomaly in the low troposphere, which weakened the temperature advection. Consequently, the decisive factors affecting the temperature tendency on the north and south sides of the jet exit area were different.

Author Contributions: Conceptualization, S.Y. and Y.L.; formal analysis, S.Y.; investigation, Y.L.; writing—original draft preparation, S.Y.; writing—review and editing, Y.L. All authors have read and agreed to the published version of the manuscript.

Funding: This research was funded by the State Key Program of the National Natural Science Foundation, grant number 41930969-3, National Key Research and Development Program of China, grant number 2019YFC0214604, and the Chinese National Natural Science Foundation, grant number 42030612, 41775096.

Institutional Review Board Statement: Not applicable.

Informed Consent Statement: Not applicable.

Data Availability Statement: All datasets presented in this study are included in the article.

Acknowledgments: The authors would like to thank Qian Huang for his help on downloading the data used in this analysis.

Conflicts of Interest: The authors declare no conflict of interest.

References

1. Madden, R.; Julian, P. Detection of a 40–50 day oscillation in the zonal wind in the tropical Pacific. *J. Atmos. Sci.* **1971**, *28*, 702–708. [CrossRef]
2. Madden, R.; Julian, P. Description of global scale circulation cells in the tropics with 40–50 day period. *J. Atmos. Sci.* **1972**, *29*, 1109–1123. [CrossRef]
3. Li, C.; Wu, P. An observational study of the 30–50 day atmospheric oscillations. Part I: Structure and propagation. *Adv. Atmos. Sci.* **1990**, *7*, 294–304. [CrossRef]
4. Jiang, X.; Li, T.; Wang, B. Structures and Mechanisms of the Northward Propagating Boreal Summer Intraseasonal Oscillation. *J. Clim.* **2004**, *17*, 1022–1039. [CrossRef]
5. Hsu, P.; Li, T.; Murakami, H. Moisture asymmetry and MJO eastward propagation in an aqua-planet general circulation model. *J. Clim.* **2014**, *27*, 8747–8760. [CrossRef]
6. Feng, J.; Li, T.; Zhu, W. Propagating and Non-Propagating MJO Events over Maritime Continent. *J. Clim.* **2015**, *28*, 8430–8449. [CrossRef]
7. Kuang, X.; Zhang, Y. Seasonal Variation of the East Asian Subtropical Westerly Jet and Its Association with the Heating Field over East Asia. *Adv. Atmos. Sci.* **2005**, *22*, 831–840.
8. Jhun, J.; Lee, E. A new East Asian winter monsoon index and associated characteristics of the winter monsoon. *J. Clim.* **2004**, *17*, 711–726. [CrossRef]
9. Ren, X.; Yang, X.; Zhou, T.; Fang, J. Diagnostic Comparison of Wintertime East Asian Subtropical Jet and Polar-front Jet: Large-scale Characteristics and Transient Eddy Activities. *Acta Meteorol. Sin.* **2011**, *25*, 21–23. [CrossRef]
10. Wang, N.; Zhang, Y. Evolution of Eurasian teleconnection pattern and its relationship to climate anomalies in china. *Clim. Dyn.* **2014**, *44*, 1017–1028. [CrossRef]
11. Kuang, X.; Zhang, Y.; Huang, Y.; Huang, D. Spatial differences in seasonal variation of the upper-tropospheric jet stream in the Northern Hemisphere and its thermal dynamic mechanism. *Theor. Appl. Climatol.* **2014**, *17*, 103–112. [CrossRef]
12. Charney, J.; Eliassen, A. A numerical method for prediction the perturbation of the middle latitude westerlies. *Tellus* **1949**, *1*, 38–55. [CrossRef]
13. Shi, Z.; Liu, X.; Liu, Y.; Sha, Y.; Xu, T. Impact of mongolian plateau versus tibetan plateau on the westerly jet over north pacific ocean. *Clim. Dyn.* **2015**, *44*, 3067–3076. [CrossRef]
14. Krishnamurti, T. The subtropical jet stream of winter. *J. Atmos. Sci.* **1961**, *18*, 172–191. [CrossRef]

15. Yang, S.; Webster, P. The effect of summer tropical heating on the location and intensity of the extratropical westerly jet streams. *J. Geophys. Res. Atmos.* **1990**, *95*, 18705–18721. [CrossRef]
16. Bjerknes, J. A possible response of the atmospheric Hadley circulation to equatorial anomalies of ocean temperature. *Tellus* **1966**, *18*, 820–829. [CrossRef]
17. Kuo, H. The motion of atmospheric vortices and the general circulation. *J. Atmos. Sci.* **1950**, *7*, 247–258. [CrossRef]
18. Ren, X.; Yang, X.; Chu, C. Seasonal variations of the synoptic-scale transient eddy activity and polar front jet over East Asia. *J. Clim.* **2010**, *23*, 3222–3233. [CrossRef]
19. Xiang, Y.; Yang, X. The effect of transient eddy on interannual meridional displacement of summer East Asian Subtropical Jet. *Adv. Atmos. Sci.* **2012**, *29*, 484–492. [CrossRef]
20. Lee, S.; Kim, H. The dynamical relationship between subtropical and eddy-driven jets. *J. Atmos. Sci.* **2003**, *60*, 1490–1530. [CrossRef]
21. Lu, R.; Lin, Z. Role of subtropical precipitation anomalies in maintaining the summertime meridional teleconnection over the Western North Pacific and East Asia. *J. Clim.* **2009**, *22*, 2058–2072. [CrossRef]
22. Guo, Y.; Wen, Z.; Wu, R.; Lu, R.; Chen, Z. Impact of tropical pacific precipitation anomaly on the East Asian upper-tropospheric westerly jet during the boreal winter. *J. Clim.* **2015**, *28*, 6457–6474. [CrossRef]
23. Xue, D.; Zhang, Y. Concurrent variations in the location and intensity of the asian winter jet streams and the possible mechanism. *Clim. Dyn.* **2017**, *49*, 37–52. [CrossRef]
24. Yu, X.; Zhang, L.; Zhou, T. The Asian Subtropical Westerly Jet Stream in CRA-40, ERA5, and CFSR Reanalysis Data: Comparative Assessment. *J. Meteorol. Res.* **2021**, *35*, 46–63. [CrossRef]
25. Jin, R.; Li, W.; Zhang, B.; Yan, C. A study of the relationship between East Asia subtropical westerly jet and abnormal Meiyu in the middle-lower reaches of the Yangtze river. *Chin. J. Atmos. Sci.* **2012**, *36*, 722–732.
26. Yao, C.; Huang, Q.; Zhu, B.; Liu, F. The 10–30-day oscillation of winter zonal wind in the entrance region of the East Asian subtropical jet and its relationship with precipitation in southern China. *Dyn. Atmos. Ocean.* **2018**, *82*, 76–88. [CrossRef]
27. Han, R.; Li, W.; Dong, M. Temporal and Spatial Characteristics of Intraseasonal Oscillations in the Meridional Wind Field over the Subtropical Northern Pacific. *Acta Meteorol. Sin.* **2010**, *24*, 276–286.
28. Barroso, J.; Zuritagotor, P. Intraseasonal Variability of the Zonal-Mean Extratropical Tropopause: The Role of Changes in Polar Vortex Strength and Upper-Troposphere Wave Breaking. *J. Atmos. Sci.* **2016**, *73*, 1383–1399. [CrossRef]
29. Yao, S.; Huang, Q.; Li, T.; Zhang, C. The intraseasonal oscillations of precipitation and circulations from January to March in 2010 in East Asia. *Meteorol. Atmos. Phys.* **2014**, *123*, 67–79. [CrossRef]
30. Yao, S.; Gong, K.; Zhao, C. Intraseasonal oscillation of the winter geopotential height in the middle latitude of the Northern Hemisphere. *J. Meteorol. Sci.* **2016**, *36*, 622–628.
31. Dee, D.; Uppala, S.; Simmons, A.; Berrisford, P.; Poli, P.; Kobayashi, S.; Andrae, U.; Balmaseda, M.; Balsamo, G.; Bauer, P.; et al. The ERA-Interim reanalysis: Configuration and performance of the data assimilation system. *Q. J. R. Meteorol. Soc.* **2011**, *137*, 553–597. [CrossRef]
32. Holton, J. *An Introduction to Dynamic Meteorology*; Academic Press: London, UK, 1992.
33. Hsu, P.; Li, T. Interactions between boreal summer Intraseasonal oscillations and synoptic-scale disturbances over the western North Pacific. Part II: Apparent heat and moisture sources and eddy momentum transport. *J. Clim.* **2011**, *24*, 942–961. [CrossRef]